

WIDE BANDGAP β -Ga₂O₃ NANOMECHANICAL RESONATORS FOR DETECTION OF MIDDLE-ULTRAVIOLET (MUV) PHOTON RADIATION

*Xu-Qian Zheng**, *Jaesung Lee*, *Subrina Rafique*, *Lu Han*,
Christian A. Zorman, *Hongping Zhao*, and *Philip X.-L. Feng**

Department of Electrical Engineering & Computer Science, Case School of Engineering,
Case Western Reserve University, Cleveland, OH 44106, USA

*Emails: xuqian.zheng@case.edu; philip.feng@case.edu

ABSTRACT

This digest paper reports on the first demonstration of suspended β -Ga₂O₃ nanostructures and nanomechanical resonators made from single-crystal β -Ga₂O₃ nanosheets or nanomembranes grown via low pressure chemical vapor deposition (LPCVD) on 3C-SiC epi-layer on Si substrate. These single-crystal β -Ga₂O₃ drumhead nanomechanical resonators offer robust multimode resonances at frequencies in the range of ~ 10 to 70 MHz. The resonators exposed to middle ultraviolet (MUV) radiation exhibit shifts in resonant frequency with a responsivity of ~ 3.8 Hz/pW.

INTRODUCTION

Among important wide bandgap oxide semiconductors, β -Ga₂O₃ is rapidly emerging as a promising candidate for future high-power electronics and transducers. Due to its very wide bandgap, $E_g \approx 4.5$ – 4.9 eV [1,2], light emitting and detecting devices made from β -Ga₂O₃ could capitalize on optoelectronic and optomechanical interactions in the middle ultraviolet (MUV) range. In addition to its wide bandgap, β -Ga₂O₃ has excellent chemical and thermal (melting point at 1820°C) stability, making it attractive for harsh environment applications. Importantly, owing to its excellent mechanical properties (Young's modulus, $E_Y \approx 300$ GPa) [3] and varieties of synthesis methods [4-6], β -Ga₂O₃ could be an excellent structural material for building MEMS and NEMS provided that it can be constructed into suspended microscale and nanoscale structures, in particular structures that can be used to access its mechanical properties. To date, use of β -Ga₂O₃ thin films has been focused on on-substrate devices, such as transistors [7]. Suspended structures of β -Ga₂O₃ that are building blocks for harnessing the optical and mechanical properties of this important crystal, have yet to be explored.

In this work, we demonstrate, for the first time, the construction of β -Ga₂O₃ nanosheets and their suspended structures, as well as the first measurement of vibrating β -Ga₂O₃ drumhead nanomechanical resonators. We perform careful characterization of the resonance properties and the demonstration of ultraviolet (UV) light sensing capability.

Table 1. Important properties of β -Ga₂O₃ crystal [7]

Melting Point [°C]	Mass Density [g/cm ³]	Bandgap [eV]	Thermal Conductivity ([100]) [W/(m·K)]
1820	5.95	4.5-4.9	13

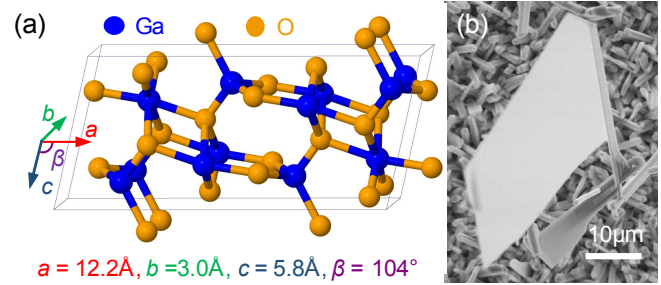


Figure 1: (a) An illustration of β -Ga₂O₃ crystal structure [7]. (b) An SEM image of a β -Ga₂O₃ nanosheet grown from a nanorod on a 3C-SiC epi-layer deposited on Si substrate.

β -Ga₂O₃ DEVICE FABRICATION

The large surface-area-to-volume ratio of a drumhead 2D resonator promises high responsivities and sensitivities to external stimuli and perturbations, making it an attractive physical sensing platform. For such promises, suspended structures are a key to enabling nanomechanical functions.

Our construction of β -Ga₂O₃ drumhead resonators starts with the low-dimensional β -Ga₂O₃ nanosheet synthesis on a 3C-SiC epi-layer on Si substrate by using a low pressure chemical vapor deposition (LPCVD) method. With a growth temperature of 950°C for 1.5 hrs, using high purity Ga pellets as source material and O₂/Ar as precursor, the formation of β -Ga₂O₃ proceeds, step by step, from β -Ga₂O₃ nanocrystals to β -Ga₂O₃ nanorods, and then nanosheets, without any foreign catalyst (Fig. 2). The as-grown nanosheets have widths of ~ 2 – 30 μ m and thicknesses of ~ 20 – 140 nm (Fig. 1b).

Using the synthesized β -Ga₂O₃ nanosheets, we fabricate suspended β -Ga₂O₃ nanostructure by employing all-dry transfer techniques (Fig. 3). With the assistance of thermal release tape, we pick up the β -Ga₂O₃ nanosheets from the as-grown samples and thermally release the flakes to a pre-fabricated 290nm-SiO₂-on-Si substrate with pre-defined circular microtrenches. Using this method, we fabricate β -Ga₂O₃ circular drumhead resonators with thicknesses of ~ 20 to ~ 80 nm and diameters of ~ 3.2 μ m and ~ 5.2 μ m.

To characterize the crystalline properties of β -Ga₂O₃ nanosheets after transfer, we examine Raman signatures of suspended β -Ga₂O₃ flakes using a 532nm laser. We find Raman modes at 143cm⁻¹, 168cm⁻¹, 199cm⁻¹, 346cm⁻¹, 416cm⁻¹, 476cm⁻¹, 631cm⁻¹, 653cm⁻¹ (Fig. 4), which match Raman modes of bulk β -Ga₂O₃ very well [8], showing high crystal quality of the β -Ga₂O₃ nanosheets after the transfer process, ensuring good β -Ga₂O₃ material properties.

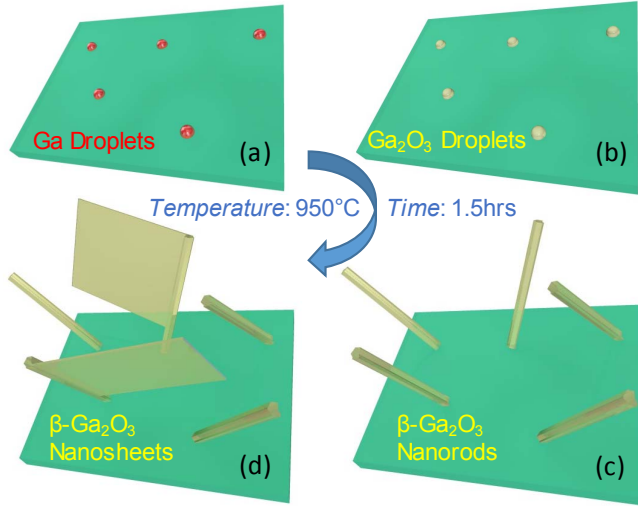


Figure 2: Schematic illustration of the LPCVD β -Ga $_2$ O $_3$ nanosheets synthesis process. While maintaining 950°C temperature in evaporated Ga and O $_2$ /Ar precursor environment for 1.5 hours, the β -Ga $_2$ O $_3$ nanosheets will form on 3C-SiC/Si substrate, in the sequence of (a) adsorption of Ga adatoms and gathering of Ga droplets, (b) formation of β -Ga $_2$ O $_3$ droplets through oxidation by O $_2$, (c) extrusion of β -Ga $_2$ O $_3$ nanorods due to supersaturation, and (d) nucleation of β -Ga $_2$ O $_3$ nanosheets from nanorod sidewalls.

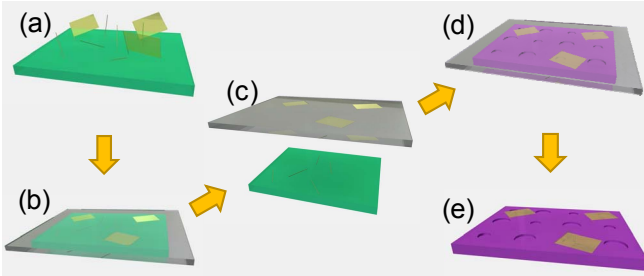


Figure 3: Illustration of the all-dry transfer process for suspended nanosheet structure fabrication. (a) Synthesized β -Ga $_2$ O $_3$ nanorods and nanosheets on 3C-SiC epi-layer. (b) Application of thermal release tape. (c) Picking up β -Ga $_2$ O $_3$ nanosheets by thermal release tape. (d) Applying tape to desired substrate and releasing nanosheets at >90°C temperature. (e) Fabricated β -Ga $_2$ O $_3$ drumhead resonators.

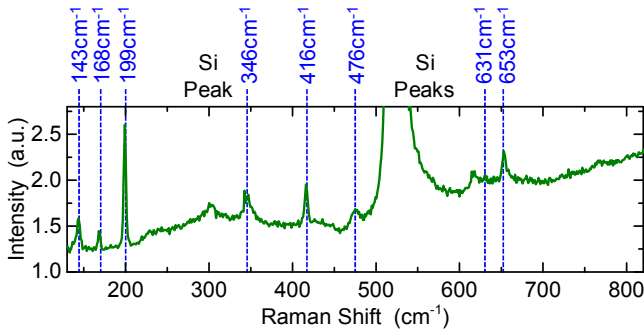


Figure 4: A typical Raman spectrum measured from a suspended β -Ga $_2$ O $_3$ drumhead device after all-dry transfer.

EXPERIMENTAL TECHNIQUES

We investigate the resonant characteristics of β -Ga $_2$ O $_3$ circular drumhead resonators by measuring flexural-mode resonances, employing a custom-built ultrasensitive laser interferometry system (Fig. 5) [9,10]. The system consists of a 633nm He-Ne laser, a set of lenses, filters and beam splitters to configure a light path, as well as a photodetector (PD, Newport 1801) and a spectrum analyzer (Agilent E4440A) to resolve the mechanical resonances of devices, a customized vacuum chamber with vacuum gauge and optical window, and a UV light source to introduce UV radiation onto the resonator. All the measurements in this work are conducted in moderate vacuum of ~ 8 to 20mTorr.

Optical interferometry is a highly effective method for ultrasmall motion detection. To introduce interferometric effect, the interfaces of resonator structural components, including suspended β -Ga $_2$ O $_3$ nanosheets and microtrench bottom surface, act as micro beam splitters and mirrors. Thus the light interference occurs when coherent light travel to the devices. The undriven Brownian motions of a β -Ga $_2$ O $_3$ nano drumhead causes variations of the air gap, generating phase modifications in the optical paths. The phase modifications create power variations of the total reflected light. By detecting this reflected light using the PD, we can measure the voltage signal and fluctuations transduced from the motions of the resonator. The spectrum analyzer is used to read out the voltage spectra of the signal from the PD, from which we can extract the resonance frequencies and quality factors (Q s) of the β -Ga $_2$ O $_3$ drumhead resonators.

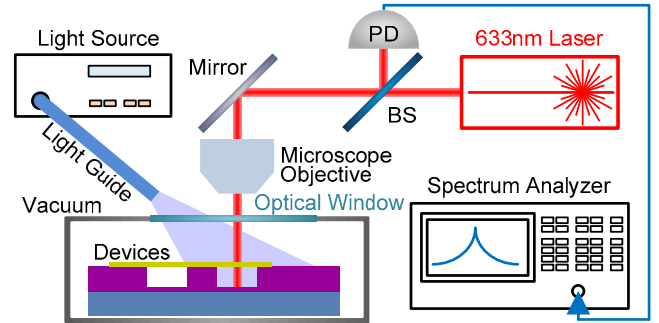


Figure 5: Customized laser interferometer with switchable UV light irradiation, for measuring the thermomechanical resonances and demonstrating resonant UV light sensing.

RESONANCE RESULTS

By measuring the undriven thermomechanical resonance spectra of the β -Ga $_2$ O $_3$ drumheads using the laser interferometry system (Fig. 5), we detect fundamental mode resonances of smaller devices ($d \approx 3.2\mu\text{m}$) and multimode resonances of larger devices ($d \approx 5.2\mu\text{m}$). Figure 6 shows a typical $d \approx 3.2\mu\text{m}$ β -Ga $_2$ O $_3$ nanosheet resonator with its fundamental mode spectrum. By fitting the spectrum using a damped simple harmonic resonator model, we extract a resonance frequency of $f = 42\text{MHz}$ and $Q = 310$. Similarly, we perform the same measurement on multiple $d \approx 3.2\mu\text{m}$ resonators and observe clear thermomechanical fundamental

mode resonances. Since the system noise floor elevates at higher frequencies, resonators with larger suspended areas are favorable for observing higher resonance modes. For all the four larger resonators with $d \approx 5.2\mu\text{m}$, we measure two or more resonance modes. Figure 7 shows a typical $d \approx 5.2\mu\text{m}$ $\beta\text{-Ga}_2\text{O}_3$ nanosheet resonator with its multimode resonance spectra. We measure the resonances up to the 3rd mode for this resonator, with resonance frequencies from 21MHz to 46MHz, and Q s around 300 to 370.

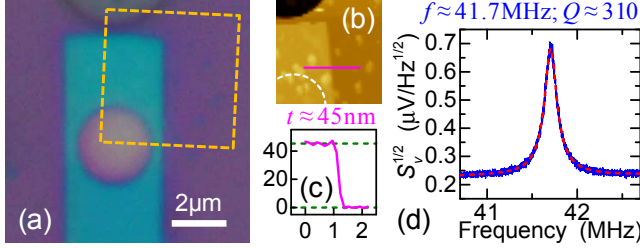


Figure 6: Optically measured resonance of a $\beta\text{-Ga}_2\text{O}_3$ nanosheet suspended over a $\sim 3.2\mu\text{m}$ diameter circular microtrench. (a) Optical device image. (b) AFM image of the dashed-line box region in (a). (c) Device thickness. (d) Device fundamental mode resonance spectrum with fitting.

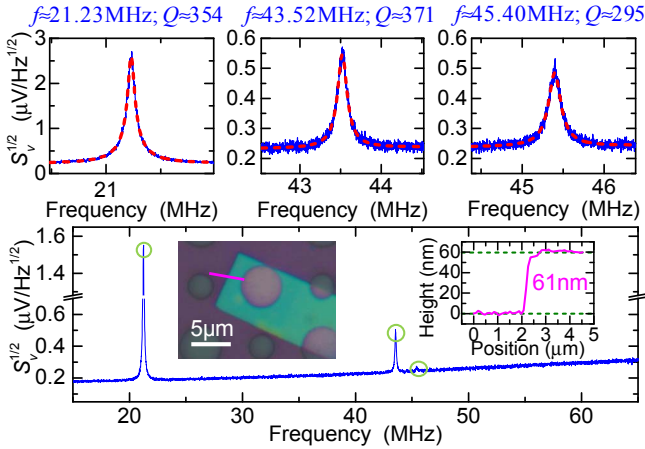


Figure 7: Optical measurement of multimode Brownian motions of a $\beta\text{-Ga}_2\text{O}_3$ drumhead resonator suspended over a $\sim 5.2\mu\text{m}$ diameter circular microtrench. Insets show the optical image of device and corresponding AFM trace. The lower panel shows wide spectrum measurement of device thermomechanical motions, with upper panels showing corresponding zoomed-in measurement of each mode.

We observe resonance frequencies in the high frequency (HF) and very high frequency (VHF) bands (10MHz to 70MHz) with Q s ranging from 100 to 420 (Fig. 8). The linear relation between the resonance frequency (f) and device thickness (t) suggests that all the $\beta\text{-Ga}_2\text{O}_3$ drumhead resonators operate in the disk regime. Therefore, an accurate measurement of resonator geometry and theoretical modeling can lead to deterministic extraction of elastic properties of $\beta\text{-Ga}_2\text{O}_3$ nanosheet, such as Young's modulus. The detailed characterization of $\beta\text{-Ga}_2\text{O}_3$ nanosheet resonator properties helps pave the way for further realization of MUV

light detection and analysis by employing such devices.

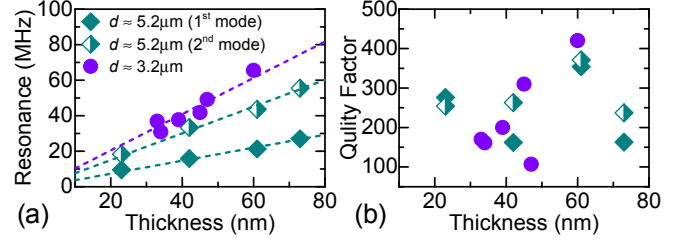


Figure 8: Summary of device (a) resonance frequencies (f), and (b) quality (Q) factors with respect to device thicknesses.

DETECTION OF MUV RADIATION

A resonator is an outstanding platform for ultrasensitive detection owing to its high responsivities and fast responses in resonance frequency shifts to external perturbations. In addition, the wide bandgap ($E_g \approx 4.5\text{--}4.9\text{eV}$) of $\beta\text{-Ga}_2\text{O}_3$ crystal makes it an excellent candidate of solar-blind UV sensing with a cut-off wavelength below ~ 250 to 260nm . Naturally, $\beta\text{-Ga}_2\text{O}_3$ should exhibit promising UV sensing functionality, utilizing its optical and mechanical properties.

We investigate the MUV (200–300nm) light detection characteristics of $\beta\text{-Ga}_2\text{O}_3$ resonators. We use a continuous UV light source of 200 to 600nm wavelength to illuminate photon radiation on $\beta\text{-Ga}_2\text{O}_3$ resonators down to the MUV regime. The light is introduced from the light source through an optical guide towards the devices (Fig. 5). We illuminate a $d \approx 5.2\mu\text{m}$ $\beta\text{-Ga}_2\text{O}_3$ resonator with intensities of $1\text{W}/\text{cm}^2$, $3\text{W}/\text{cm}^2$ and $5\text{W}/\text{cm}^2$ from the optical guide tip, which corresponds to incident power levels of 37nW, 111nW and 185nW on the suspended device area, respectively. Figure 9 shows the detection of MUV light for a $\beta\text{-Ga}_2\text{O}_3$ drumhead resonator with a thickness of $\sim 42\text{nm}$. By periodically switching on and off the MUV light, we measure the frequency responses of the resonator due to MUV light illumination. The results show a linear response between frequency shift and incident light power on device, with an average responsivity of $-3.8\text{Hz}/\text{pW}$ upon light radiation down to MUV wavelength (Fig. 9g). The extracted Q s also exhibit similar linear relation with incident light intensity (Fig. 9h), even though not as clear as the frequency shift.

The frequency downshift with MUV radiation could be explained by photothermal effect. With 4.5–4.9eV bandgap, $\beta\text{-Ga}_2\text{O}_3$ will absorb light below 250–260nm wavelength, generating heat from the photothermal absorption. The elevated temperature of $\beta\text{-Ga}_2\text{O}_3$ will expand the nanosheet, softening the resonator and causing a frequency downshift. To further solidify the explanation, the SiO_2 layer has a much higher bandgap ($\sim 9\text{eV}$), exhibiting negligible absorption above 200nm wavelength (limited by the light source). In addition, SiO_2 layer can mechanically isolate the thermal expansion of the UV-absorbing Si layer, while the oxide's low thermal conductivity also makes it a good heat barrier between the bottom Si and the $\beta\text{-Ga}_2\text{O}_3$. The photothermal expansion of $\beta\text{-Ga}_2\text{O}_3$ layer could be well isolated from parasitic effects in the resonator, contributing majority of

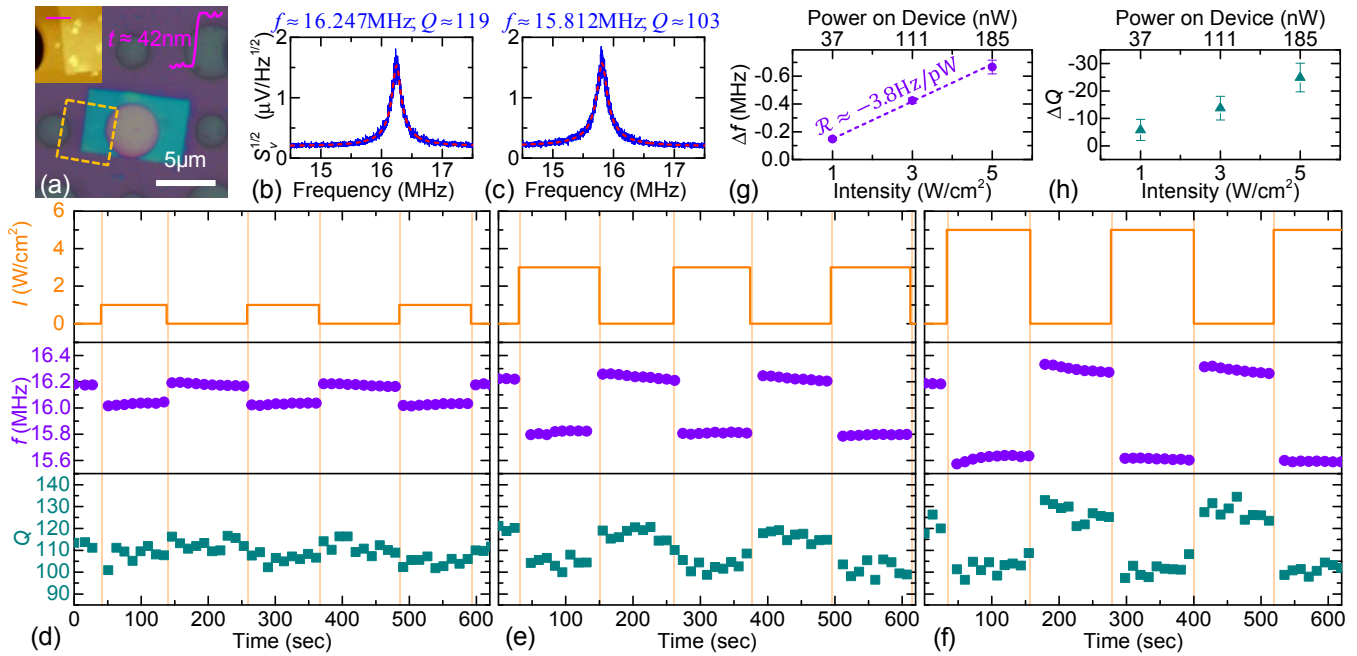


Figure 9: Middle-ultraviolet (MUV) light detection using a $\sim 5.2 \mu\text{m}$ diameter $\beta\text{-Ga}_2\text{O}_3$ nanomechanical drumhead resonator. (a) Device optical and AFM images with measured thickness. Device's fundamental mode thermomechanical resonance (b) without light radiation and (c) with $3 \text{ W}/\text{cm}^2$ (11 nW on device) light radiation. Fundamental thermomechanical resonance frequency and Q factor with cycling illumination of (d) $1 \text{ W}/\text{cm}^2$, (e) $3 \text{ W}/\text{cm}^2$, and (f) $5 \text{ W}/\text{cm}^2$ intensity (37 nW , 11 nW , and 185 nW light power on device, respectively). (g) Frequency shifts and (h) Q changes under different source light intensities.

perturbation to the device. Thus the frequency downshift of the $\beta\text{-Ga}_2\text{O}_3$ drumhead resonator is mainly due to the MUV light photothermal effects in the $\beta\text{-Ga}_2\text{O}_3$ nanosheet.

CONCLUSIONS

This study provides the first demonstration and a quantitative resonance characteristics assessment of the nanoscale $\beta\text{-Ga}_2\text{O}_3$ drumhead resonators, and paves the way for future nanomechanical devices engineering with this new crystalline material. The demonstration of MUV detection reveals the potential of using $\beta\text{-Ga}_2\text{O}_3$ nanoresonators as ultrasensitive solar-blind ultraviolet ($< 280 \text{ nm}$) sensors in harsh environment conditions (*i.e.*, high temperatures), for applications including target detection and acquisition, flame detection, biomedicine, and environmental monitoring.

ACKNOWLEDGEMENTS

We thank financial support from the U.S. Department of Energy (DOE) EERE Grant (DE-EE0006719) and the Great Lakes Energy Institute (GLEI) ThinkEnergy Fellowship.

REFERENCES

- [1] M. R. Lorenz, J. F. Woods, R. J. Gambino, "Some electrical properties of the semiconductor $\beta\text{-Ga}_2\text{O}_3$ ", *J. of Phys. & Chem. of Solids*, vol. 28, 403-404, 1967.
- [2] N. Ueda, H. Hosono, R. Waseda, H. Kawazoe, "Anisotropy of electrical and optical properties in $\beta\text{-Ga}_2\text{O}_3$ single crystals", *Applied Physics Letters*, vol. 71, 933-935, 1997.
- [3] M.-F. Yu, M. Z. Atashbar, X. Chen, "Mechanical and electrical characterization of $\beta\text{-Ga}_2\text{O}_3$ nanostructures for sensing applications", *IEEE Sensors Journal*, vol. 5, 20-25, (2005).
- [4] S. Rafique, L. Han, C. A. Zorman, H. Zhao, "Synthesis of wide bandgap $\beta\text{-Ga}_2\text{O}_3$ rods on 3C-SiC-on-Si", *Crystal Growth & Design*, vol. 16, 511-517, 2016.
- [5] S. Rafique, L. Han, H. Zhao, "Synthesis of wide bandgap Ga_2O_3 ($E_g \sim 4.6\text{--}4.7 \text{ eV}$) thin films on sapphire by low pressure chemical vapor deposition", *Physica Status Solidi A*, vol. 213, 1002-1009, 2016.
- [6] S. Rafique, L. Han, A. T. Neal, S. Mou, M. J. Tadjer, R. H. French, H. Zhao, "Heteroepitaxy of N-type $\beta\text{-Ga}_2\text{O}_3$ thin films on sapphire substrate by low pressure chemical vapor deposition", *Applied Physics Letters*, vol. 109, 132103, 2016.
- [7] W. S. Hwang, A. Verma, H. Peelaers, V. Protasenko, S. Rouvimov, H.G. Xing, A. Seabaugh, W. Haensch, C. van de Walle, Z. Galazka, M. Albrecht, R. Fornari, D. Jena, "High-voltage field effect transistors with wide-bandgap $\beta\text{-Ga}_2\text{O}_3$ nanomembranes", *Applied Physics Letters*, vol. 104, 203111, 2014.
- [8] C. Kranert, C. Sturm, R. Schmidt-Grund, M. Grundmann, "Raman tensor elements of $\beta\text{-Ga}_2\text{O}_3$ ", *Scientific Reports*, vol. 6, 35964, 2016.
- [9] Z. Wang, J. Lee, P. X.-L. Feng, "Spatial mapping of multimode Brownian motions in high-frequency silicon carbide microdisk resonators", *Nature Communications*, vol. 5, 5158, 2014.
- [10] J. Lee, Z. Wang, K. He, J. Shan, P. X.-L. Feng, "High frequency MoS_2 nanomechanical resonators", *ACS Nano*, vol. 7, 6086-6091, 2013.